Molecular Therapy
Nucleic Acids
Original Article

Exosome-mediated inhibition of microRNA-449a promotes the amplification of mouse retinal progenitor cells and enhances their transplantation in retinal degeneration mouse models

Chen Jun Guo,[2,3] Xiu Li Cao,[1] Yu Fei Zhang,[1] Kang Yi Yue,[1] Jing Han,[2] Hong Yan,[4] Hua Han,[3] and Min Hua Zheng[1]

[1]Department of Medical Genetics and Developmental Biology, Fourth Military Medical University, Xi'an 710032, Shaanxi, China; [2]Department of Ophthalmology, Tangdu Hospital, Fourth Military Medical University, Xi'an 710038, Shaanxi, China; [3]Department of Biochemistry and Molecular Biology, Fourth Military Medical University, Xi'an 710032, Shaanxi, China; [4]Shaanxi Eye Hospital, Xi'an People's Hospital (Xi'an Fourth Hospital), Affiliated Guangren Hospital, School of Medicine, Xi'an Jiaotong University, Xi'an 710004, Shaanxi, China

Inherited and age-related retinal degenerations are the commonest causes of blindness without effective treatments. Retinal progenitor cells (RPCs), which have the multipotency to differentiate into various retinal cell types, are regarded as a promising source of cell transplantation therapy for retinal degenerative diseases. However, the self-limited expansion of RPCs causes difficulty in cell source supply and restrict its clinical treatment. In this work, we found that inhibition of microRNA-449a (miR-449a) in RPCs can promote proliferation and inhibit apoptosis of RPCs, partially through upregulating Notch signaling. Further optimization of transduction miR-449a inhibitor into RPCs by endothelial cell-derived exosomes can promote the survival of RPCs transplanted *in vivo* and reduce cell apoptosis in retinal degeneration mouse models. In summary, these studies have shown that exosome-miR-449a inhibitor can effectively promote the expansion of RPCs *in vitro* and enhance transplanted RPCs survival *in vivo*, which might provide a novel intervention strategy for retinal degenerations in the future.

INTRODUCTION

Retinal degenerative diseases such as retinitis pigmentosa (RP) or age-related macular degeneration (AMD) are the main causes of currently untreatable blindness.[1–3] In most cases, retinal degenerations (RDs) are characterized by a slow progression over several years with a continuous loss of photoreceptors and progressive loss in vision, and eventually progress to blindness.[1,4] Photoreceptors, including rods and cones, are light receptors in the eye, and the death of photoreceptors leads to irreversible vision defects without curable treatment at present.[5–7] Stem cell transplantation holds great promise as a potential therapeutic approach for retinal degenerative diseases.[8,9] Since photoreceptors are derived from retinal progenitor cells (RPCs) at embryonic and early postnatal stages, RPCs are attractive as a potential cell source of repopulating the retina with rods and cones in patients with RD.[10,11] RPCs are a class of neural progenitor cells having the capacity to self-renew and differentiate into retinal neurons and glia.[12,13] Several studies claimed that transplantation of RPCs in RD models could protect the retina from continuous photoreceptor apoptosis.[14–16] However, one of the existing shortages of this therapy is the self-limited expansion of RPCs *in vitro*.[17] Although this characteristic diminishes the risk of uncontrolled proliferation and carcinogenesis, it also brings the problem of insufficient donor cells, which has limited RPC transplantation to be used in clinical practice. In this study, we tried to find a method to enhance the expansion of RPCs *in vitro* and promote transplanted RPC survival *in vivo*.

MicroRNAs (miRNAs) are a family of small, noncoding RNA molecules that play important roles in many biological processes, including cell proliferation, differentiation, apoptosis, and organ development and homeostasis.[18–20] miRNAs exert their function by negatively regulating gene expression through direct binding to the 3′ UTR of a target gene mRNA, which induces mRNA cleavage or translational repression.[21,22] Previous research has reported miRNA-449a (miR-449a) regulates proliferation and apoptosis of retinoblastoma cells.[23] miR-449a belongs to the miR-34 family and encodes the highly conserved miRNAs, including miR-449a, miR-449b, and miR-449c.[24,25] Besides retinoblastoma, the studies of miR-449a also revealed its function in glioblastoma, colorectal cancer, and cell multiciliogenesis.[26–28] However, the biological functions of miR-449a in normal retina and RPCs are still unknown.

In this study, we investigate the function of miR-449a in RPCs and optimized transportation of miR-449a inhibitor into RPCs by

Received 29 July 2022; accepted 11 February 2023;
https://doi.org/10.1016/j.omtn.2023.02.015.

Correspondence: Min-Hua Zheng, Department of Medical Genetics and Developmental Biology, Fourth Military Medical University, Xi'an 710032, China.
E-mail: zhengmh@fmmu.edu.cn
Correspondence: Hua Han, Department of Biochemistry and Molecular Biology, Fourth Military Medical University, Chang-Le Xi Street #169, Xi'an 710032, China.
E-mail: huahan@fmmu.edu.cn

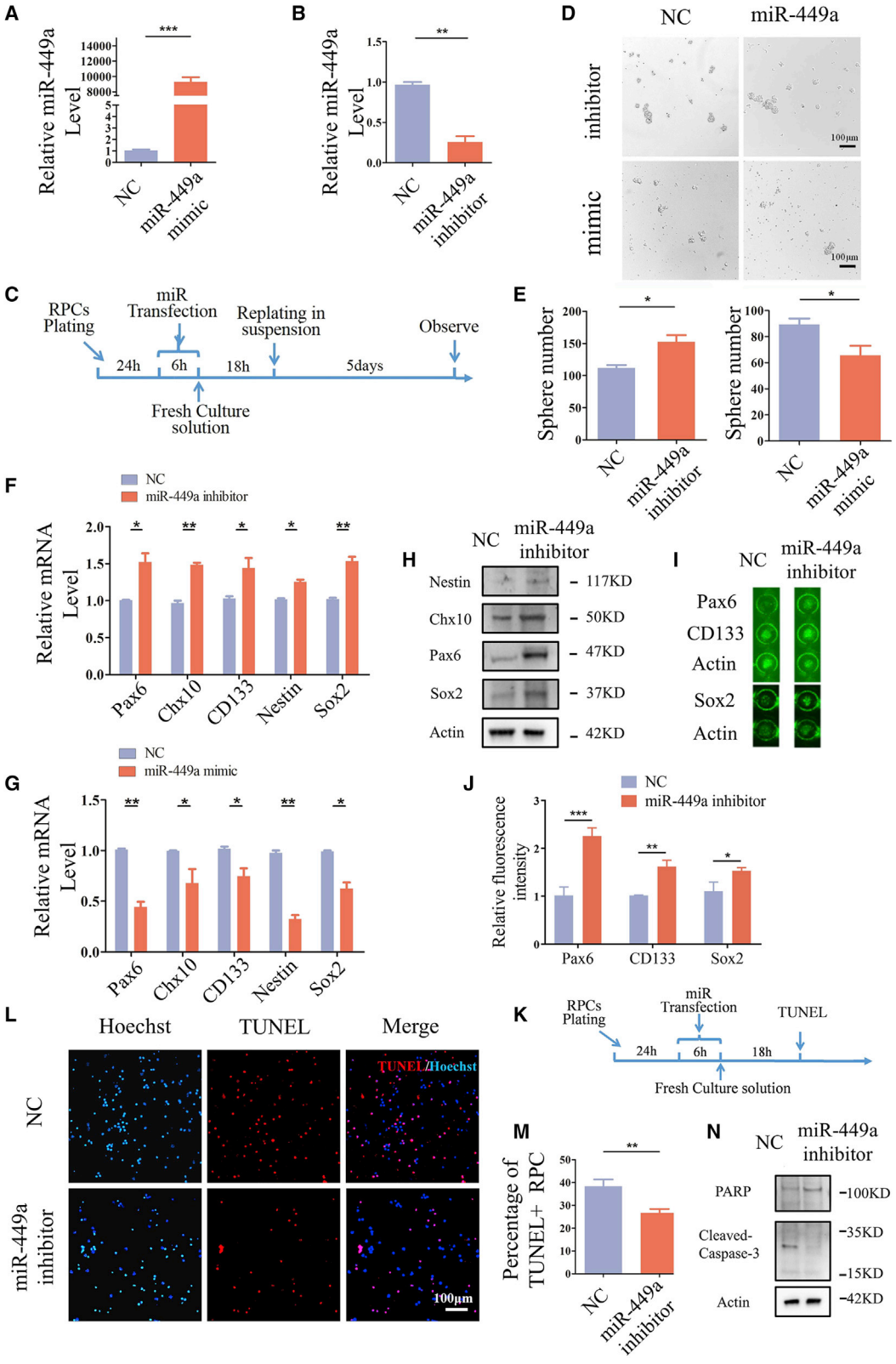

(legend on next page)

endothelial cell-derived exosomes. We found that exosome-mediated miR-449a inhibition could enhance stemness, promote proliferation, and resist apoptosis of RPCs. Moreover, miR-449a regulates RPCs partially through Notch signaling, with Notch1 been identified as a direct target gene. We also determined that transplantation of RPCs with miR-449a inhibitor packed by exosome reduced the apoptosis of retinal cells both in NMDA-induced and Pde6b mutant RD models. These results might provide a novel intervention strategy for patients with rod-cone dystrophy and other retinal degenerative diseases in the future.

RESULTS

The inhibition of miR-449a promotes the self-renewal of RPCs and inhibits their apoptosis

Previous research has shown that miR-449a is expressed in neural progenitor cells (NPCs) and retinoblastoma.[23,29] To test whether miR-449a is also expressed in RPCs, we cultured mouse RPCs and tested the expression of several miRNAs, with miR-449a most abundant in RPCs among these miRNAs (Figure S1). Primary RPCs were extracted from embryonic day 17.5 (E17.5) embryonic retina, cultured to form neurospheres and identified by immunofluorescent staining of RPC markers Pax6, Nestin, and Sox2 (Figures S2A and S2B). The expression level of miR-449a was decreased during RPC sphere formation, whereas it was increased during RPCs' induced differentiation *in vitro* (Figures S2C and S2D). Next, to investigate whether miR-449a regulates the self-renewal of RPCs, we transfected cultured RPCs with synthetic miR-449a mimics and inhibitors. RPC neurospheres were dissociated and replated under adherent condition for 24 h and transfected with miR-449a mimics or inhibitors, with control oligonucleotides respectively. We first confirmed the overexpression or downregulation of miR-449a 24 h after transfections. As shown by RT-qPCR results (Figures 1A and 1B), miR-449a level was significantly lower in the miR-449a inhibitor-transfected group and was intensively higher in miR-449a mimic-transfected group, compared with the control group respectively. The transfected RPCs were then detached and replated in suspension for 5 days to observe the formation of neurospheres (Figures 1C and 1D). As shown in Figure 1D, the inhibition of miR-449a increased the sphere number of RPCs compared with the control group, and upregulation of miR-449a decreased the sphere number of RPCs compared with the control group. Statistical results were consistent with this observation (Figure 1E). In addition, we tested the expression of stemness markers by RT-qPCR 24 h after transfection. As shown in Figures 1F and 1G, the mRNA levels of *Pax6*, *Chx10*, *CD133*, *Nestin*, and *Sox2* were all upregulated in the miR-449a inhibitor group compared with the control group, and were downregulated in the miR-449a mimic group (Figures 1F and 1G). These changes in stemness markers were confirmed when their mRNA levels were tested 5 days after transfection (Figures S3A–S3D). Due to the limited amount of primary cultured RPCs, we first used in-cell western blotting to detect the protein levels of stemness markers. As shown in Figure 1I, the protein levels of Pax6, CD133, and Sox2 were all upregulated in the miR-449a inhibitor group compared with the control group (Figures 1I and 1J). After enlargement of the amount of primary culture, we finally acquired sufficient protein samples to perform western blotting and verified the increased protein levels of stemness markers under miR-449a inhibition (Figure 1H). All these results indicated that downregulation of miR-449a promoted the self-renewal of RPCs, whereas upregulation of miR-449a led to reduced RPC stemness.

We further investigate whether miR-449a affects the apoptosis of RPCs (Figure 1K). Terminal deoxynucleotidyl transferase-mediated dUTP nick end labeling (TUNEL) labeling showed that the number of $TUNEL^+$ cells was decreased after miR-449a inhibition compared with the control group (Figure 1L). Statistics results also showed that the proportion of apoptotic RPCs was significantly reduced under miR-449a inhibition (Figure 1M). Furthermore, we also performed western blotting to test the cleavage of Caspase-3 and poly (ADP-ribose) polymerase (PARP), and the results showed that miR-449a inhibition significantly suppresses cleavage of Caspase-3 and its substrate PARP, verifying reduced apoptosis under miR-449a inhibition (Figure 1N). Therefore, the above results indicate that inhibition of miR-449a can protect RPCs from apoptosis.

miR-449a inhibition enhances the proliferation of RPCs and has no obvious effect on their differentiation

Next, we explored whether inhibition of miR-449a affects the proliferation and differentiation of RPCs. We detected RPC proliferation by Ki67 immunostaining 24 h after miR-449a inhibitor transfection (Figure 2A). The results showed that $Ki67^+$ RPCs were increased in the miR-449a inhibitor group compared with the control group (Figures 2B and 2C). Furthermore, the *Ki67* mRNA level was also increased in RPCs transfected with miR-449a inhibitor compared with control (Figure 2D).

To study miR-449a's function in RPC differentiation, we used serum-containing medium with added retinoic acid to culture RPCs for 7 days after transfection (Figure 2E). Then, after 7 days, we examined $Rhodopsin^+$ rod cell and $Cone\text{-}arrestin^+$ cone cell by immunofluorescence staining. As shown in Figures 2F and 2G, there is no obvious

Figure 1. The inhibition of miR-449a promotes the self-renewal of RPCs and inhibits their apoptosis

(A and B) RT-qPCR analysis of miR-449a expression in RPCs after mimic or inhibitor transfection. (C) Diagram of RPCs sphere assay after miRNA transfection. (D) Brightfield microscope of RPCs sphere after miRNA transfections. (E) RPCs sphere number after miRNA transfection. (F and G) RT-qPCR analysis of stemness markers *Pax6*, *Chx10*, *CD133*, *Nestin*, and *Sox2* in RPCs after miRNA transfection. (H) Western blot analysis of stemness markers Nestin, Chx10, Pax6, and Sox2 after miRNA transfection. (I) Detection of protein levels of stemness markers Pax6, CD133, and Sox2 by in-cell western blot after miR-449a inhibitor transfection. (J) Results of in-cell western blot in (I). (K) Diagram of RPCs TUNEL staining after miRNA transfection. (L) TUNEL staining on RPCs after miR-449a inhibitor transfection. (M) Results of RPCs TUNEL staining. (N) Western blot analysis of cleaved-Caspase-3 and PARP protein after miRNA transfection. Experiments were performed at least in triplicate, and the results are shown as the mean ± SD. Student's t test was used to analyze the data. *$p < 0.05$, **$p < 0.01$, ***$p < 0.001$.

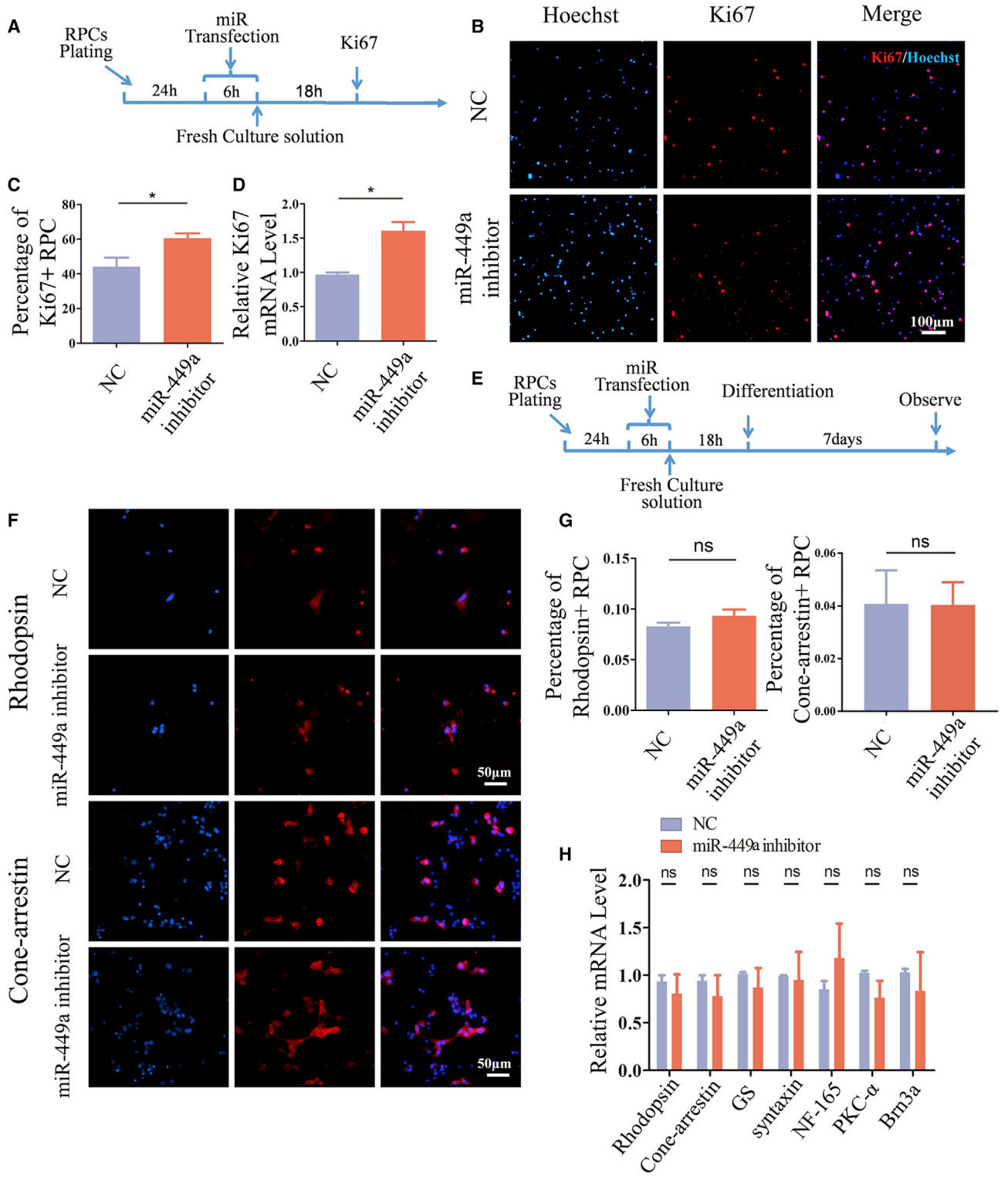

Figure 2. miR-449a inhibition enhances the proliferation of RPCs and has no obvious effect on their differentiation

(A) Diagram of RPCs Ki67 immunostaining after miRNA transfection. (B) Ki67 immunostaining of RPCs after miR-449a inhibitor transfection. (C) The percentage of Ki67^{+} RPCs in (B). (D) RT-qPCR analysis of *Ki67* expression in RPCs after miR-449a inhibitor transfection. (E) Diagram of RPC differentiation assay after miRNA transfection. (F)

(legend continued on next page)

difference in the percentages of differentiated photoreceptors in total cells between the miR-449a inhibitor group and the control group (Figures 2F and 2G). In addition, mRNA expression of the markers of seven mature retinal cell types were tested by RT-qPCR, including *glutamate synthetase* (GS) for Muller's glia, *syntaxin* for amacrine cells, *NF165* for horizontal cells, *PKC-α* for bipolar cells, *Brn3a* for ganglion cells, as well as *Rhodopsin* and *Cone-arrestin* for photoreceptors.[30,31] The results showed that mRNA expression levels of all seven markers have no significant difference between the miR-449a inhibitor group and control group (Figure 2H). In summary, all these data demonstrate that the inhibition of miR-449a enhances the proliferation of RPCs and has no obvious effect on their differentiation.

miR-449a regulates the stemness, proliferation, and apoptosis of RPCs partially by modulation of Notch signaling

Notch signaling has been documented to play pivotal roles in the regulation of RPC stemness and differentiation.[32–34] To determine whether miR-449a's functions on stemness, proliferation, and apoptosis of RPCs is achieved by Notch signaling, we first observed the phenotypes of RPCs after inhibiting the Notch pathway by gamma-secretase inhibitor (GSI). We confirmed the efficiency of Notch inhibition by testing its canonical downstream genes *Hes1* and *Hes5* in RPCs (Figure 3A). Then we found that the sphere number of RPCs incubated with GSI is reduced compared with the control group treated with DMSO (Figures 3B and 3C). Furthermore, RT-qPCR testing the stemness markers showed that *Pax6*, *Chx10*, *CD133*, *Nestin*, and *Sox2* were all downregulated after the inhibition of Notch signaling (Figure 3D), and western blot analysis showed that the protein levels of Pax6, Chx10, and Sox2 were also decreased under GSI treatment (Figure 3E). As shown in Figures 3F and 3G, the percentage of $Ki67^+$ cells in the GSI group decreased compared with that of the control group. Correspondingly, the mRNA expression level of *Ki67* in the GSI group was lower than that of the control group (Figure 3H). On the other hand, the percentage of TUNEL-positive cells in the GSI group increased compared with that of the control group (Figures 3I and 3J). Next, to investigate whether miR-449a regulates the stemness, proliferation, and apoptosis of RPCs through the Notch signaling pathway, we transfected miR-449a inhibitor and added GSI simultaneously. The experiment showed that the inhibition of Notch signaling by GSI can partially reduce the expression of stemness-related genes upregulated by miR-449a inhibition (Figure 3K). Taken together, these findings suggest that miR-449a regulates the stemness, proliferation, and apoptosis of RPCs partially through modulation of Notch signaling.

miR-449a modulates Notch signaling by directly regulating the 3′ UTR of Notch1 mRNA

To identify miR-449a-mediated downstream regulators for stemness, proliferation, and apoptosis of RPCs, the target genes of mir-449a were selected from the shared genes from miRNA target gene predictions, including TargetScan 6.2 (http://www.targetscan.org), miRDB (https://www.mirdb.org/), and RNA22 version 2.0 (https://www.rna-seqblog.com/rna22-version-2-o-mirna-mre-predictions/). As shown in Figure 4A, we took intersections from three databases, and then we screened out 17 genes that meet at least one of these filter conditions, including cell proliferation, neuron development, nervous system, and neurogenesis, and that have expression in the visual system or retina. Notch1 is found in the list (Figure 4A). Therefore, to find the interaction between miR-449a and Notch1, we first detected the expression of *Notch1* and its downstream genes *Hes1* and *Hes5* by RT-qPCR after the inhibition or overexpression of miR-449a in the RPCs. The results showed that *Notch1* and its downstream genes increased under the inhibition of miR-449a, compared with the control group (Figure 4B). In contrast, *Notch1* and its downstream genes significantly decreased in miR-449a-overexpressing RPCs (Figure 4C). To further confirm the physical interaction and post-transcriptional regulation on the 3′ UTR fragment of *Notch1* by miR-449a, we used genome DNA PCR to clone the mouse *Notch1* 3′ UTR containing the putative binding site of miR-449a and constructed the appropriate luciferase reporter plasmids including the normal binding site and mutated binding site, respectively (Figure 4D). As shown in Figure 4E, we used transient transfection to co-introduce luciferase plasmid containing the 3′ UTR region of *Notch1* or the corresponding mutated region with the miR-449a mimic into HEK293T cells. The dual-luciferase reporter assay showed that the normalized luciferase activity decreased in the miR-449a mimic and *Notch1* 3′ UTR reporter co-transfection group, whereas this effect was abolished when the binding site of miR-449a was mutated (Figure 4E). Collectively, these results demonstrated that *Notch1* is a direct target of miR-449a.

Endothelia-derived exosomes significantly reduce the apoptosis of cultured RPCs

Next, in order to improve the transfection efficacy and reduce the toxicity of transfect regent on RPCs, we aimed to deliver miR-449a inhibitor into RPCs by exosomes. Previously, we have shown that endothelial cell-derived exosomes could protect cultured neural stem cells from apoptosis and maintain their stemness.[35] Here, we used the bEnd.3 cell line-derived exosomes to investigate whether endothelia-derived exosomes also have an effect on cultured RPCs. As shown in Figure 5A, the exosome-specific proteins CD9, CD63, and ALIX were detected in bEnd.3 cell line-derived exosomes. Transmission electron microscopy showed the extracted exosomes with typical vesicle morphology (Figure 5B). Nanoparticle tracking analysis (NTA) determined the size of the vesicles (Figure 5C). Next, RPCs' proliferation, stemness, and apoptosis were observed after co-incubation with the bEnd.3 cell-derived exosomes. The expression of stemness-related genes was mostly stable in RPCs after co-incubation, except for *Chx10*, which showed a decrease (Figure 5D). In addition, there is no obvious difference in RPC proliferation between the co-incubation group and control group shown by *Ki67* expression

Rhodopsin and Cone-arrestin immunostaining on differentiated RPCs after miR-449a inhibitor transfection. (G) The percentages of $Rhodopsin^+$ and $Cone\text{-}arrestin^+$ cells in (F). (H) RT-qPCR analysis of retinal cell markers in differentiated RPCs. Experiments were performed at least in triplicate, and the results are shown as the mean ± SD. Student's t test was used to analyze the data. *$p < 0.05$; **$p < 0.01$; ***$p < 0.001$; ns, not significant.

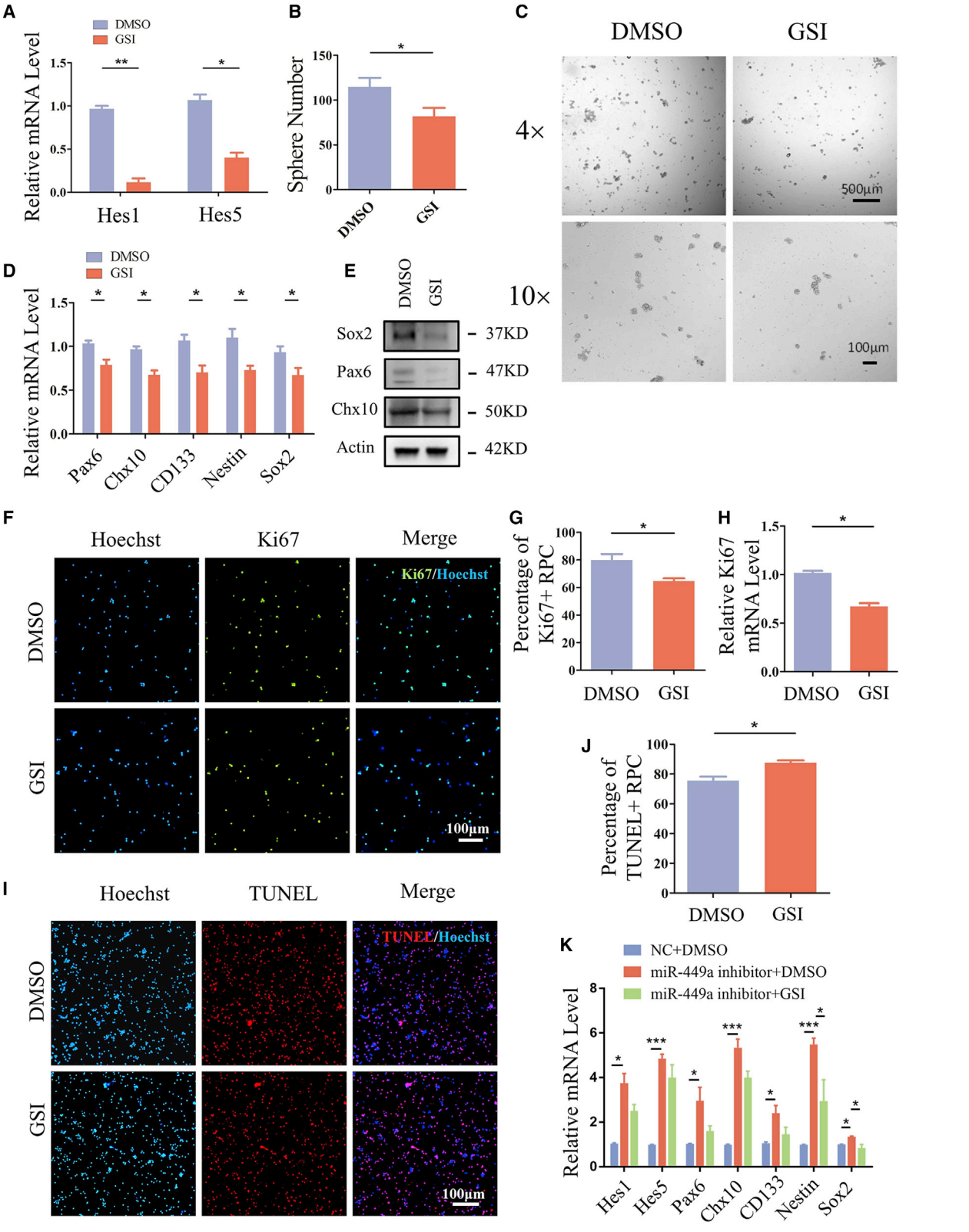

(legend on next page)

(Figure 5E). Most importantly, TUNEL staining results showed that endothelial cell-derived exosome incubation could significantly reduce the apoptosis of RPCs (Figures 5F and 5G), and this effect on inhibiting RPC apoptosis gradually enhanced with increased concentrations of exosomes (Figure S4).

Exosome-mediated inhibition of miR-449a promotes the stemness and proliferation of RPCs and reduces their apoptosis

We further confirmed that the level of miR-449a was relatively low in bEnd.3-derived exosomes (Figure S5A), and there was no significant increase in miR-449a level in RPCs incubated with exosomes compared with PBS (Figure S5B). Therefore, bEnd.3-derived exosomes can be used as appropriate transport vesicle of miR-449a inhibitor. Next, we transfected bEnd.3 cells with miR-449a inhibitor and then extracted exosomes and incubated these miR-449a inhibitor-enriched exosomes with RPCs. We first tested whether these exosomes could effectively carry miR-449a inhibitor into RPCs. As shown in Figure 6A, the RT-qPCR results showed that the expression of miR-449a in RPCs incubated with exosome-miR-449a (Exo-miR-449a) inhibitor was significantly downregulated compared with the control group. This result verified that miR-449a inhibitor was effectively transported into RPCs by bEnd.3 cell-derived exosomes. Then we analyzed the proliferation, stemness, and apoptosis of RPCs between control (PBS or Exo-negative control [NC] incubated) groups and Exo-miR-449a inhibitor-incubated group respectively. The results showed that the expression of *Ki67* was significantly upregulated after Exo-miR-449a inhibitor incubation (Figure 6B), indicating that proliferation of RPCs was enhanced on Exo-miR-449a inhibitor treatment. In addition, the mRNA expressions of stemness genes *Chx10*, *Sox2*, and *Nestin* were upregulated in Exo-miR-449a inhibitor group (Figure 6E), and the in-cell western blotting result confirmed the elevated protein level of Sox2 in the Exo-miR-449a inhibitor group compared with the control groups (Figures 6C and 6D). These results indicate that incubation with exosome-enriched miR-449a inhibitor could enhance the stemness of RPCs. Moreover, the TUNEL staining result showed that the percentage of TUNEL$^+$ RPCs was decreased in the Exo-miR-449a inhibitor group compared with the control groups (Figures 6F and 6G), suggesting that exosomes with miR-449a inhibitor could reduce the apoptosis of RPCs. Together, these data demonstrate that exosome-mediated inhibition of miR-449a not only promotes the stemness and proliferation but also reduces the apoptosis of RPCs.

The transplantation of miR-449a-inhibited RPCs can reduce the apoptosis of retinal cells in RD models

In order to determine whether Exo-miR-449a-treated RPCs have a protective effect *in vivo*, we transplanted Exo-miR-449a inhibitor-treated RPCs by subretinal injection into degenerated retina models (Figure 7A). First, we utilized a pharmacological RD model by subretinal injection of NMDA.[36] About 2 weeks after injection, TUNEL$^+$ cells were mainly located in the outer nuclear layer (ONL) of the retina, indicating toxic effects on photoreceptors (white arrows in Figure 7B). Then, for transplantation, RPCs were pre-stained with DiIC18(3), 1,1'-dioctadecyl-3,3,3',3'tetra- methylindocarbocyanine perchlorate (DiI). Next, we subretinally injected Exo-NC or Exo-miR-449a inhibitor-treated RPCs into NMDA-injured RD mice and observed the following neuronal apoptosis in retina. As shown in Figures 7B and 7D, after NMDA injection, apoptotic cells appeared in the retina compared with the PBS injection group. After injection of Exo-miR-449a inhibitor-treated RPCs, the number of TUNEL$^+$ cells in neural retina was reduced compared with the NMDA group (Figures 7B and 7D). In addition, the injection of Exo-NC-treated RPCs also reduced cell apoptosis, probably due to endothelia-derived exosomes in transplanted cell suspension. We next utilized a genetic RD model. The Pde6b mutant mouse has been shown to have a significant photoreceptor reduction in the ONL of retina (Figure S6), due to continued photoreceptor apoptosis initiating around postnatal day 16 (P16).[37] To test the effect of Exo-miR-449a inhibitor-treated RPC transplantation on the inherited RD model, PBS, Exo-NC, or Exo-miR-449a inhibitor-treated RPCs were injected subretinally into P15 Pde6b mouse retina. After 2 weeks, we observed more DiI-positive cells in the Exo-miR-449a inhibitor RPC group compared with the Exo-NC RPC group (Figures 7C and 7E), and the number of TUNEL$^+$ cells in the ONL of retina was less in the Exo-miR-449a inhibitor RPC group, compared with the control PBS or Exo-NC RPC group (Figures 7C and 7E). Finally, to clarify the effect of RPC transplantation on visual improvement, we first made an acute retinal injury model through NMDA subretinal injection and then detected electroretinogram (ERG) 2 weeks after transplantation (Figures 7F–7J). In ERG results, the amplitudes of both a-wave and b-wave in maximal response (Max) increased in the eyes transplanted with Exo-miR-449a inhibitor-treated RPCs (Figures 7F–7H), compared with control eyes (NMDA + PBS injected group and Exo-NC-treated RPCs transplantation group). The b-wave amplitudes in scotopic 0.01 ERG (rod response, Figures 7F and 7J) and photopic 3.0 ERG (cone response, Figures 7F and 7I) were also higher in the eyes transplanted with Exo-miR-449a inhibitor-treated RPCs compared with control eyes (NMDA + PBS injected group and Exo-NC-treated RPCs transplantation group). Based on the above results, exosome-contained miR-449a inhibitor can maintain the survival of transplanted RPCs, reduce the apoptosis of retinal cells, and improve ERG responses of photoreceptors in retina degeneration models.

Figure 3. miR-449a regulates the stemness, proliferation, and apoptosis of RPCs partially by modulation of Notch signaling

(A) RT-qPCR analysis of *Hes1* and *Hes5* expression in RPCs after GSI treatment. (B) RPC sphere numbers after GSI treatment. (C) Brightfield microscopy of RPC spheres treated with GSI or DMSO. (D) RT-qPCR analysis of stemness markers in RPCs treated with GSI or DMSO. (E) Western blot analysis of stemness markers Sox2, Pax6, and Chx10 after GSI treatment. (F) Ki67 immunostaining of RPCs treated with GSI or DMSO. (G) Results of Ki67$^+$ RPCs in (F). (H) RT-qPCR analysis of *Ki67* expression in RPCs after GSI treatment. (I) TUNEL staining of RPCs treated with GSI or DMSO. (J) Results of TUNEL$^+$ RPCs in (I). (K) RT-qPCR analysis of stemness markers in RPCs after miRNA transfection and GSI or DMSO treatment. GSI, 75 μM; DMSO, 75 μM. Experiments were performed at least in triplicate, and the results are shown as the mean ± SD. $^*p < 0.05$, $^{**}p < 0.01$, $^{***}p < 0.001$.

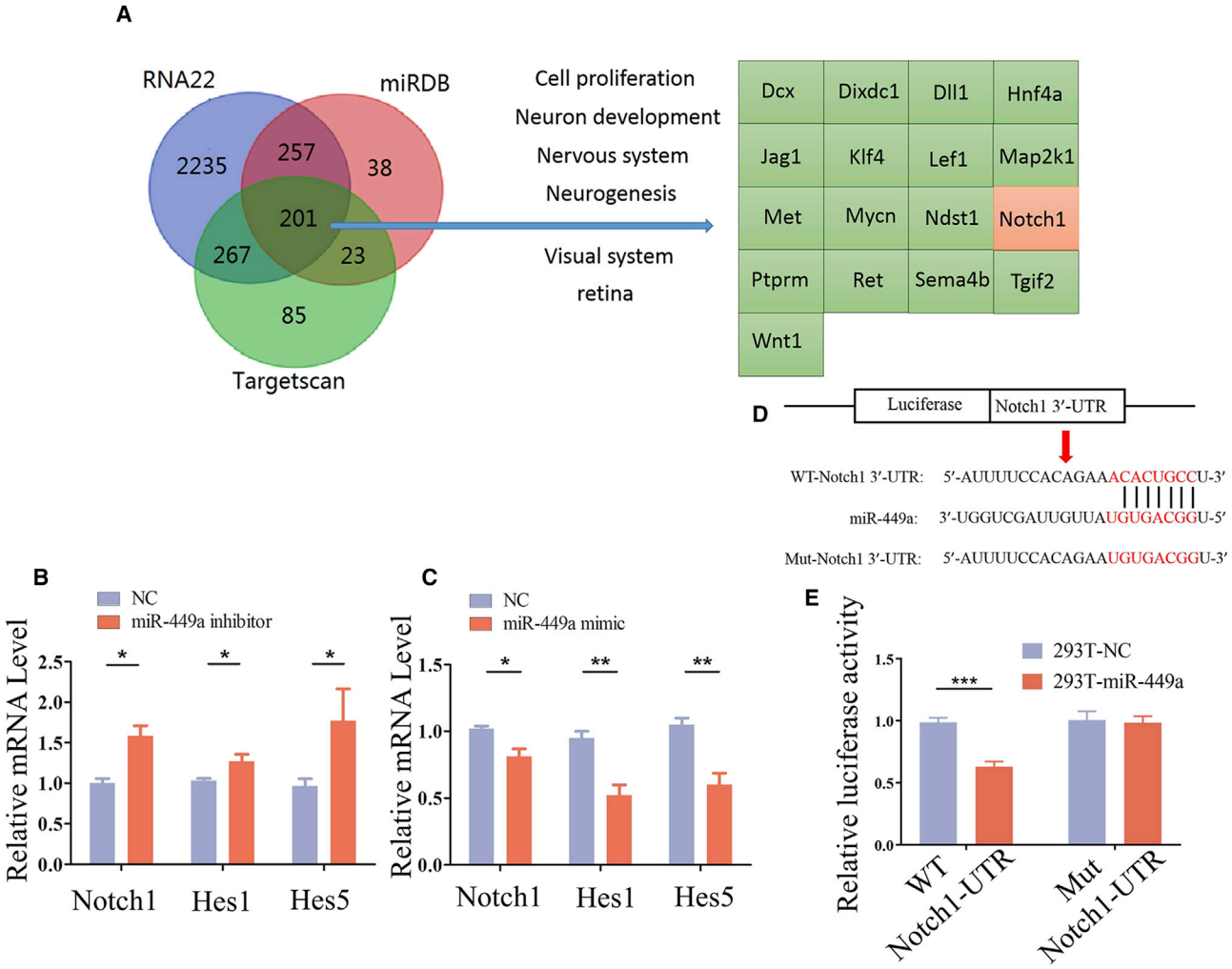

Figure 4. miR-449a modulates Notch signaling by directly regulating the 3′ UTR of *Notch1* mRNA

(A) The screening of target genes of miR-449a from the Venn diagram intersection genes predicted by RNA22, miRDB, and TargetScan database. (B) RT-qPCR analysis of *Notch1*, *Hes1*, and *Hes5* in RPCs transfected with miR-449a inhibitor or NC. (C) RT-qPCR analysis of *Notch1*, *Hes1*, and *Hes5* mRNA expression in RPCs transfected with miR-449a mimic or NC. (D) miR-449a and its potential binding sequence in the 3′ UTR of mouse *Notch1*. The wild-type and mutant *Notch1* 3′ UTR were constructed into pGL3 reporter vectors. (E) Relative luciferase assay was performed 48 h after miRNA and reporter vector transfection. Experiments were performed at least in triplicate, and the results are shown as the mean ± SD. Student's t test was used to analyze the data. *$p < 0.05$, **$p < 0.01$, ***$p < 0.001$.

DISCUSSION

RPCs are a kind of multipotent cells that have capacities of self-renewing and differentiation into various retinal cells. Therefore, RPCs have significant therapeutic potential for retina degenerative diseases. However, one of the main issues facing RPC transplantation is the shortage of sufficient donor cells due to the limited proliferative capacity of RPCs. Although previous research reported extended passaging of RPCs under hypoxic conditions,[38] the hypoxic treatment might have multifaceted effects on progenitor cells. Therefore, simple and efficient methods for amplifying RPCs are still urgently needed. In this study, we found that exosome-mediated inhibition of miR-449a promotes expansion and inhibits apoptosis of RPCs *in vitro*, enhances the survival of RPCs, and reduces cell apoptosis after subretinal RPC transplantation in RD mouse models.

Notch signaling is an evolutionarily conserved pathway in multicellular organisms that regulates cell fate during development and maintains the homeostasis of adult tissues. In retinal development, Notch signaling also plays pivotal roles in RPCs maintenance and retinal cell specification and differentiation. Several studies suggest that Notch signaling maintains RPC stemness, and inhibition of Notch signaling reduces the proliferation of RPCs.[32–34] Our previous work has shown that conditional knockout of RBP-J in the mouse retina, which blocks the canonical Notch signaling, promotes the differentiation of RPCs into photoreceptors and ganglion cells.[31] In this study, we found

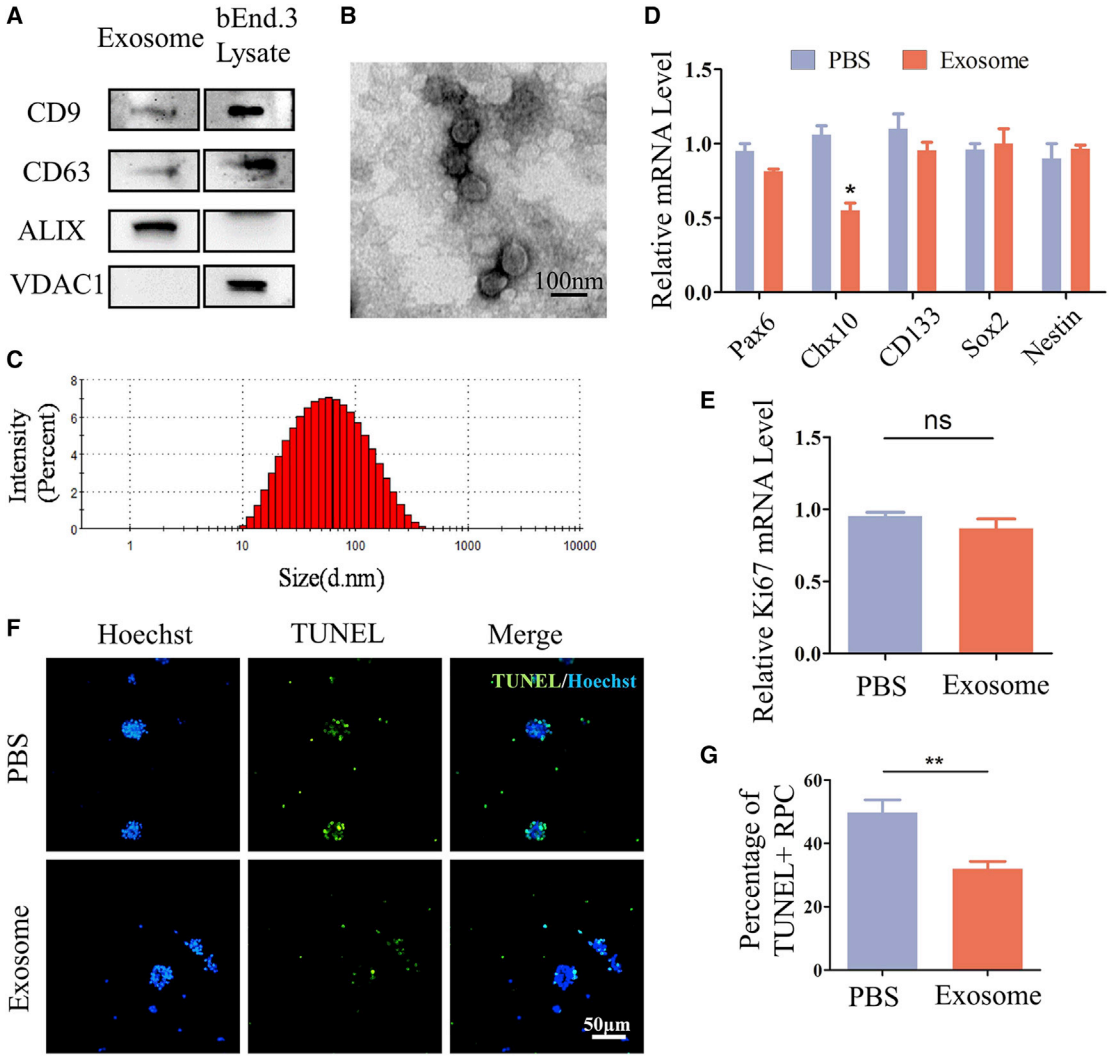

Figure 5. Endothelia-derived exosomes significantly reduce the apoptosis of cultured RPCs

(A) Western blot of exosome markers CD9, CD63, and ALIX. (B) Transmission electron micrographs of bEnd.3-derived exosomes. Scale bar, 100 nm. (C) NTA showed the particle size of bEnd.3-derived exosomes. (D) RT-qPCR analysis of stemness markers in RPCs after 24-h incubation with exosomes compared with PBS. (E) RT-qPCR analysis of *Ki67* expression in RPCs after 24-h incubation with exosomes compared with PBS. (F) TUNEL staining of RPCs co-cultured with exosomes (10 μg/mL) or PBS. Scale bar, 50 μm. (G) Statistics of TUNEL$^+$ RPCs in (F). Experiments were performed at least in triplicate, and the results are shown as the mean ± SD. Student's t test was used to analyze the data. *$p < 0.05$; **$p < 0.01$; ns, not significant.

that the blockade of Notch signaling by GSI also inhibits RPC proliferation and reduces their stemness. Moreover, miR-449a inhibition in RPCs leads to activation of Notch signaling, promotes the stemness of RPCs, and enhances their proliferation. Further analysis confirmed *Notch1* as a direct target gene negatively regulated by miR-449a. Therefore, the miR-449a-Notch axis regulates RPCs and might provide a novel strategy to amplify RPCs *in vitro* and to promote transplanted RPC maintenance *in vivo* during retinal pathology.

miR-449a has previously been reported as a key regulator of mitotic spindle orientation in the developing cerebral cortex.[29] Analysis of miR-34/449 knockout mouse embryos demonstrates significant spindle misorientation phenotypes in cortical neural progenitors, resulting in an excess of radial glia cells at the expense of intermediate progenitors and a significant delay in neurogenesis.[29] In retinoblastoma, miR-449a and miR-449b have an inhibitory effect on retinoblastoma by inhibiting proliferation and promoting apoptosis of tumor cells when these miRNAs are overexpressed. This study suggests that these miRNAs could serve as viable therapeutic targets for retinoblastoma treatment. In our study on RPCs, we also found that inhibition of miR-449a promotes RPCs proliferation and reduces their apoptosis. However, whether miR-449a regulates RPCs through affecting the mitotic spindle of RPCs requires further study.

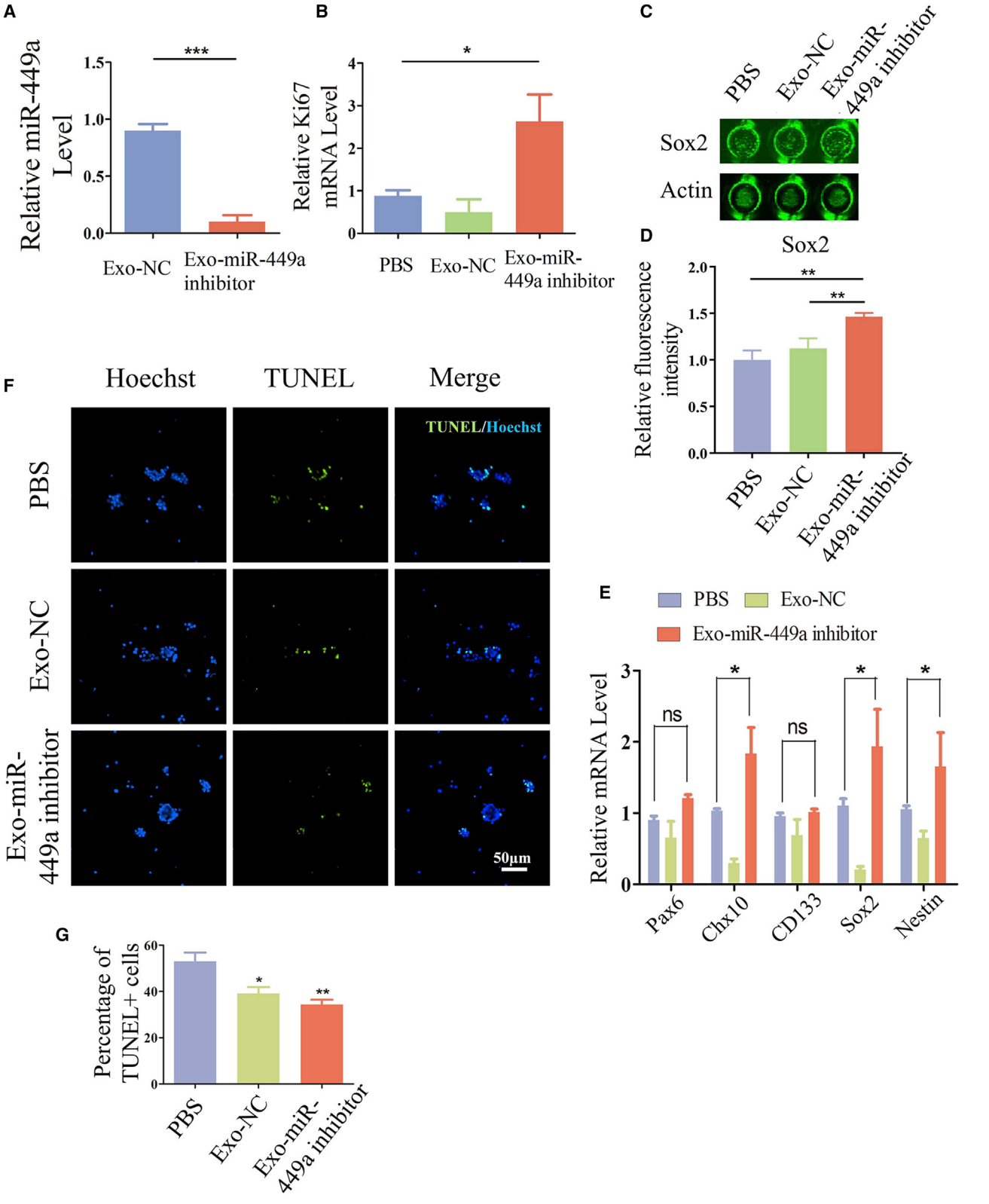

(legend on next page)

In the present study, we used the endothelial cell-derived exosomes to pack miR-449a inhibitor molecules into RPCs, instead of lipofectamine agents, which cause more RPC apoptosis. Exosomes have been reported to act as a transport pathway to transfer miRNAs from one cell to another.[39] Our previous study showed that endothelial cell-derived exosomes significantly promote stemness and reduce apoptosis of cultured neural stem cells (NSCs).[35] In this study, endothelial cell-derived exosomes also alleviate RPC apoptosis. Taken together, using endothelial cell-derived exosomes loaded with miR-449a inhibitor promotes proliferation and inhibits apoptosis of RPCs *in vitro*.

For *in vivo* study, we transplanted RPCs into the subretinal cavity of RD mouse models to observe the survival of graft RPCs and the protective effect on RD progress. We used an acute injury-induced RD model via subretinal injection of NMDA and a genetically deficient mouse model of Pde6b mutation. Our data show that subretinal injection of Exo-miR-449a inhibitor-treated RPCs can alleviate apoptosis and promote donor RPC survival at the same time, and partially retain the amplitudes of ERG, indicating a functional improvement. However, our transplantations failed to curb photoreceptor apoptosis, and there was no behavioral evidence of visual improvement. In the future, various modifications on transplantation intervention, including the amount of Exo-miR-449a inhibitor-treated RPCs and the timing of transplantation in the RD pathological process, will be needed to optimize the effect of improved visual function after transplantation. In addition, previous literature has revealed that transplanted RPCs can reduce photoreceptor apoptosis in RD by differentiating into neurons, secreting factors, or improving microenvironment.[14–16] In this study, whether Exo-miR-449a inhibitor also regulates RPC secretion, improves the microenvironment, and facilitates RPC differentiation *in vivo*, in addition to increasing the survival of transplanted RPCs by promoting their proliferation and inhibiting their apoptosis, is also a question worthy of further study.

MATERIALS AND METHODS

Reagent

Antibodies against Ki67 (ABclonal, A2094, rabbit), Pax6 (BioLegend, 901301, rat), Nestin (BD, 556309, rat), Sox2 (Abcam, ab97959, rabbit), CD133 (Invitrogen, PA5-38014, rabbit), Chx10 (Invitrogen, PA5-116119, rabbit), Rhodopsin (Invitrogen, MA5-11741, mouse), Cone-arrestin (Millipore, MAAB15282, rabbit), cleaved-Caspase-3 (Cell Signaling Technology, #9661, rabbit), PARP (Cell Signaling Technology, #9532, rabbit), CD9 (Abcam, ab92729, rabbit), CD63 (Abcam, ab217345, rabbit), Alix (Abcam, ab186429, rabbit), Vdac1 (Abcam, ab15895, rabbit), and β-actin (GeneTex, GTX11003, mouse) were used. TUNEL assay kit was purchased from Roche. Opti-MEM, neurobasal medium, Lipofectamine 2000, and LTX were obtained from Promega. Fetal bovine serum (FBS) was from Gibco.

Cell culture

bEnd.3 cells were cultured in DMEM containing 10% FBS and placed in a constant-temperature environment of 5% CO_2 at 37°C, and were passaged every 3 days. RPCs were isolated from retina of E17.5 C57BL/6 mouse embryos.[40,41] Embryos were taken from E17.5 pregnant mice, and eyeballs were separated under a microscope. The retina tissue was stripped and collected within the PBS droplets. The collected retina tissue was digested with the EDTA-containing trypsin, and then was filtered using a strainer. After centrifugation, the cells were resuspended in Neurobasal medium supplemented with 2% B27 (Gibco), 1% N2 (Gibco), 10 μg/mL basic fibroblast growth factor (bFGF) (R&D Systems), 5 μg/mL EGF (R&D Systems), 1% penicillin, 1% streptomycin, and 2.5 μg/mL heparin, and plated in ultra-low-attachment culture plates (Corning, NY). Half the volume of the medium was replaced with fresh medium on the third day of the culture, and the number of neurospheres was counted on the fifth day after the setting of the culture. In cell passaging, spheres were dispersed into single cells by digesting with Accutase (Invitrogen, CA).

Cell transfection

The miR-449a mimic and inhibitor were synthesized by Ribobio and dissolved in diethylpyrocarbonate (DEPC) water to a final concentration of 20 μM. The cultured RPCs were digested and plated on poly-L-lysine (PLL) (Sigma-Aldrich, PA)-coated 24-well plates. miRNAs were transfected by using Lipofectamine LTX (Invitrogen, CA) according to the manufacturer's instructions.

RPC sphere formation assay

At 18 h after transfection, RPCs were collected, digested with Accutase for 5 min, and centrifuged at 200 × *g* for 5 min. Cells were counted and plated at a density of 4×10^3 cells/well into ultra-low-attachment 24-well plate. Half the volume of the medium was replaced with fresh medium on the third day of the culture, and the number of RPC spheres was counted under a microscope (Eclipse Ti, Nikon, Japan) on the fifth day after the setting of the culture.

RPC differentiation assay

At 18 h after transfection, the RPC digests were plated on PLL-coated 24-well plates. The culture medium had 10% FBS and DMSO-solubilized all-*trans*-retinoic acid (Sigma-Aldrich, SHANGHAI, China) added at a final concentration of 100 ng/mL.[42] In addition, N2 and

Figure 6. Exosome-mediated miR-449a inhibitor promotes the stemness and proliferation and reduces the apoptosis of RPCs

(A) RT-qPCR analysis of miR-449a expression in RPCs after 24-h incubation with exosome-NC or Exo-miR-449a inhibitor. (B) RT-qPCR analysis of *Ki67* expression in RPCs after 24-h incubation with exosome-NC or Exo-miR-449a inhibitor compared with PBS. (C) In-cell western blot of Sox2 protein in RPCs after 24-h incubation with exosome-NC or Exo-miR-449a inhibitor compared with PBS. (D) Statistic results of in-cell western blotting in (C). (E) RT-qPCR analysis of stemness markers in RPCs after 24-h incubation with exosome-NC or Exo-miR-449a inhibitor compared with PBS. (F) TUNEL staining of RPCs after incubation for 24 h with exosome-NC or Exo-miR-449a inhibitor compared with PBS. (G) Results of $TUNEL^+$ RPCs in (F). Experiments were performed at least in triplicate, and the results are shown as the mean ± SD. *$p < 0.05$; **$p < 0.01$; ***$p < 0.001$; ns, not significant.

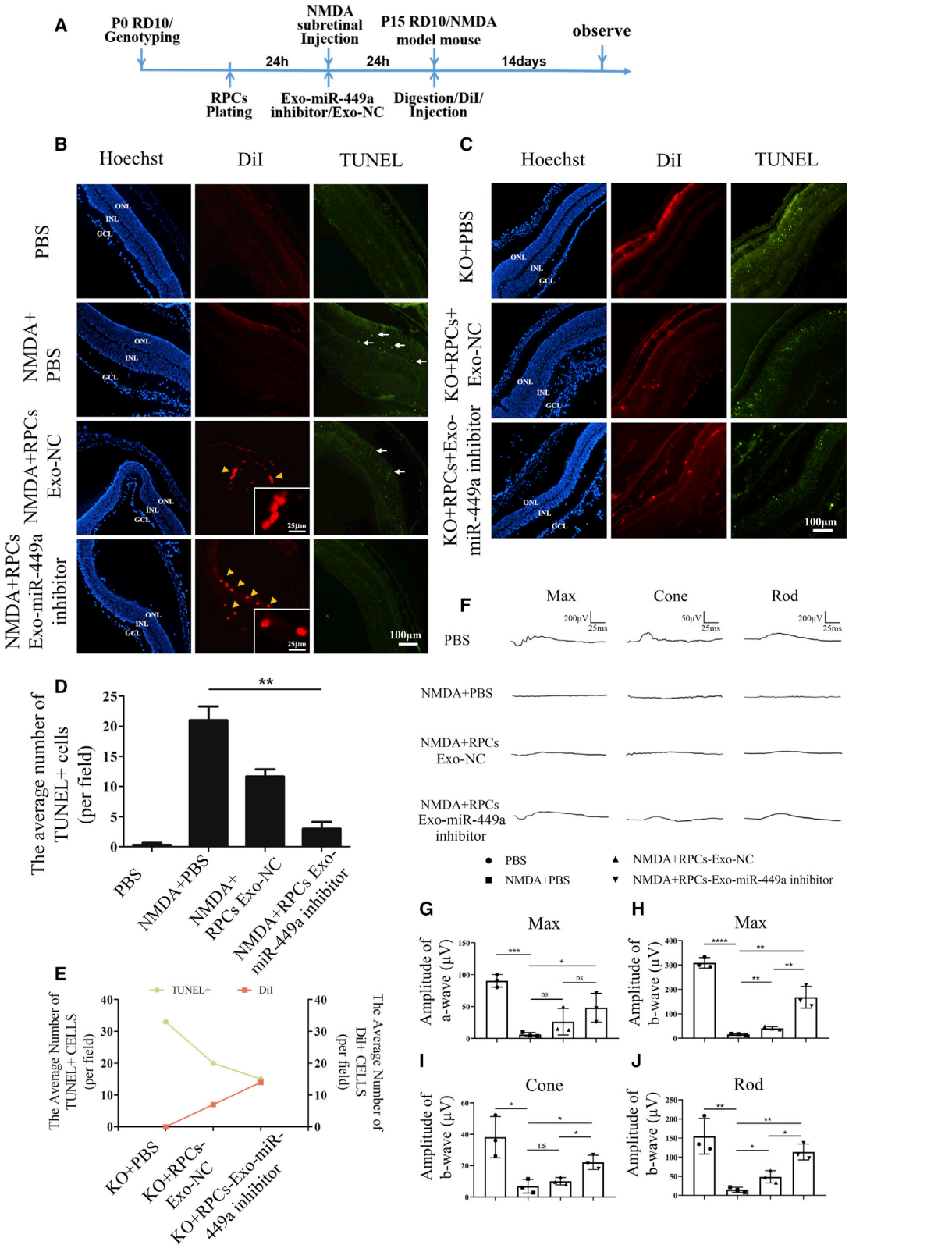

(legend on next page)

B27 supplements were removed. After 7 days of culture, differentiated RPCs were analyzed.

TUNEL

TUNEL staining utilized the DeadEnd Fluorometric TUNEL System kit (Promega, WI) and followed the manufacturer's instructions. RPCs were fixed with 4% paraformaldehyde for 30 min, and then incubated with a solution containing 0.1% Triton X-100 and 0.1% trisodium citrate for 20 min. Then transferase buffer, recombinant terminal deoxynucleotidyl transferase and biotin-labeled dUTP (biotin-16-dUTP) were applied onto the cells and incubated for 1 h at 37°C. After washing with PBS, RPCs were incubated with Avidin-Cy3 for 1 h at room temperature. Then the nuclei were counterstained with Hoechst 33342 and observed under a fluorescence microscope (Eclipse Ti, Nikon, Japan).

Cellular immunofluorescence staining

The RPC spheres were digested and plated onto PLL-coated slides. The supernatant was removed and RPCs were fixed with 4% PFA for 15 min. Then cells were washed, blocked with PBS solution containing 0.1% Triton X-100 and 0.3% BSA for 15 min, and incubated with primary antibodies anti-Rhodopsin (1:500), anti-Cone-arrestin (1:500), anti-Pax6 (1:300), anti-Nestin (1:500), anti-Sox2 (1:500), and anti-Ki67 (1:500) at 4°C for 12 h. Then, cells were incubated with the secondary antibodies for 2 h at room temperature. After washing with PBS, the nuclei were stained with Hoechst 33342 and observed under a fluorescence microscope (Eclipse Ti, Nikon, Japan).

RNA isolation and RT-qPCR

Total RNA of cells or exosomes were isolated using TRIzol reagent according to manufacturer's instructions. RNA content was measured using Nanodrop-2000. cDNA was synthesized using 1 μg of RNA using the PrimeScript RT Reagent Kit Perfect Real Time or miScript II RT Kit. To determine the amount of target miRNA and mRNA levels, we used Fast SYBR Green Chemistry for fluorescence real-time qPCR on Bio-Rad C1000 thermal cycler. All the primers are listed in Table 1.

Western blot and in-cell western

Proteins of exosomes and cells were extracted with radio immunoprecipitation assay (RIPA) lysate containing a protease inhibitor cocktail. The protein concentration was measured by a bicinchoninic acid (BCA) kit (Pierce). Samples were boiled for 10 min and separated by 12% sodium dodecyl SDS-PAGE and transferred to a polyvinylidene fluoride (PVDF) membrane. The PVDF membrane was blocked with Tris-buffered saline with Tween 20 (TBST) containing 5% skim milk for 1 h. The PVDF membrane was incubated in the primary antibody at 4°C for 12 h. Primary antibodies anti-Nestin, anti-Pax6, anti-Chx10, anti-Sox2, anti-cleaved-Caspase-3, anti-PARP, anti-CD9, anti-CD63, anti-Alix, and anti-Vdac1 were diluted according to the manufacturers' specifications. After washing the membrane with Tris-buffered saline, the horseradish peroxidase (HRP) secondary antibodies were incubated for 2 h at room temperature. The PVDF membranes were observed through a chemoluminescence system. For in-cell western blotting, RPCs were plated on PLL-coated 96-well plates. RPCs were fixed using 4% paraformaldehyde, and then were blocked and perforated with PBS solution containing 0.1% Triton X-100 and 0.3% BSA for 15 min. RPCs were incubated with primary antibodies at 4° C for 12 h, followed by IgG (H + L) DyLight 680 Conjugated second antibodies (Cell Signaling Technology, USA). The intensity of fluorescence was measured using a LI-COR Odyssey system.

Target gene prediction and luciferase reporter assay

The target genes of miR-449a were determined from the union of miRNA target predictions from TargetScan 6.2 (http://www.targetscan.org), miRDB (http://www.mirdb.org/), and RNA22 version2.0 (https://www.rna-seqblog.com/rna22-version-2-0-mirna-mre-predictions/). The 3′ UTR fragment of *Notch1* was amplified by PCR from mouse genomic DNA and inserted into the pGL3 reporter vector.[43] For the reporter assay, HEK293T cells were plated and transfected with pGL3-*Notch1*-3′ UTR or pGL3-mutant-*Notch1*-3′ UTR vectors, 20 μM miR-449a mimics, or negative control. Renilla luciferase plasmid was co-transfected as a control. The two luciferase activities were measured by a dual-luciferase system (Promega, USA).

Exosome isolation and characterization

Exosomes were extracted from bEnd.3 cell supernatant by PEG6000 using the same method as before.[35] In brief, the cell supernatant collected by centrifugation at 3,000 × *g* for 30 min was incubated with PEG6000 solution overnight at 4°C. Next day, the mixture was centrifuged at 12,000 × *g* for 1 h, the supernatant was removed, and the pellet was dissolved in PBS. The exosomes were observed by electron microscopy and the exosome markers were detected by western blotting. The proposed exosomal purity was determined by particle size analysis.

Figure 7. The transplantation of miR-449a-inhibited RPCs can reduce the apoptosis of retinal cells in RD models

(A) Diagram of RPC subretinal injection and observation in NMDA-induced retina injury model and RD10 mice. (B) TUNEL staining of NMDA-injured retina subretinally injected with RPCs incubated with exosome-NC, or RPCs incubated with Exo-miR-449a inhibitor. Red fluorescent signal represents DiI-labeled transplanted cells, indicated by yellow arrowheads. Green fluorescent signal represents TUNEL$^+$ retinal cells, indicated by white arrows. (C) TUNEL staining of retina sections from RD10 mice subretinally injected with PBS, RPCs incubated with exosome-NC, or RPCs incubated with Exo-miR-449a inhibitor. (D) Results of TUNEL$^+$ cells in (B). (E) Correlation analyses between apoptotic cells and the number of surviving DiI$^+$ cells. (F) Representative ERG waveforms of each group in response to light flashes. Max, scotopic 3.0 ERG (maximal response); Cone, photopic 3.0 ERG (cone response); Rod, scotopic 0.01 ERG (rod response). (G and H) Quantitative analysis of a-wave and b-wave amplitudes in scotopic 3.0 ERG. (I) Quantitative analysis of b-wave amplitudes in photopic 3.0 ERG. (J) Quantitative analysis of b-wave amplitudes in scotopic 0.01 ERG. Experiments were performed at least in triplicate, and the results are shown as the mean ± SD. ONL, outer nuclear layer; INL, inner nuclear layer; GCL, ganglion cell layer. *$p < 0.05$; **$p < 0.01$; ***$p < 0.001$; ****$p < 0.0001$; ns, not significant.

Table 1. The sequences of primers for mRNA detection

mRNA	Forward (5′-3′)	Reverse (5′-3′)
Pax6	TACCAGTGTCTACCAGCCAAT	TGCACGAGTATGAGGAGGTCT
Chx10	CGATTCCGAAGATGTTTCCTCC	ATCTGGGTAGTGGGCTTCATT
CD133	ACTGAGAAATCCCCTACTGAAGT	GGCCTGTTTCGGCTTTCCTT
Nestin	TGAAAAGTTCCAGCTGGCTGT	AGTTCTCAGCCTCCAGCAGAGT
Sox2	GCGGAGTGGAAACTTTTGTCC	CGGGAAGCGTGTACTTATCCTT
Notch1	GATGGCCTCAATGGGTACAAG	TCGTTGTTGTTGATGTCACAGT
Hes1	AAAGACGGCCTCTGAGCAC	GGTGCTTCACAGTCATTTCCA
Hes5	AGTCCCAAGGAGAAAAACCGA	GCTGTGTTTCAGGTAGCTGAC
Ki67	CAGTACTCGGAATGCAGCAA	CAGTCTTCAGGGGCTCTGTC
Rhodopsin	TCACCACCACCCTCTACACA	TGATCCAGGTGAAGACCACA
Cone-arrestin	AAGAAGACTAGCTCCAATGGGA	AACAAGGACGACTCCATCAATG
Glutamine Synthetase	TGAACAAAGGCATCAAGCAAATG	CAGTCCAGGGTACGGGTCTT
syntaxin	AGAGATCCGGGGCTTTATTGA	AATGCTCTTTAGCTTGGAGCG
NF165	ACAGCTCGGCTATGCTCAG	CGGGACAGTTTGTAGTCGCC
PKC-α	CCCATTCCAGAAGGAGATGA	TTCCTGTCAGCAAGCATCAC
Brn3a	CACTCTCGCACAACAACATGA	TTCTTCTCGCCGCCGTTGA
β-actin	CATCCGTAAAGACCTCTATGCCAAC	ATGGAGCCACCGATCCACA

Animals

B6.CXB1-Pde6b RD10/J mice were purchased from Jackson Laboratory (Bar Harbor, ME, United States). RD10 mice were maintained on the C57BL/6 background and genotyped by PCR with tail DNA as a template. Mice were maintained in a 12-h light and 12-h dark cycle in a specific pathogen-free (SPF) facility. All animal experiments were performed according to the protocols approved by the Animal Experiment Administration Committee of the Fourth Military Medical University.

Cell therapy on NMDA injury model and genetic injury model

NMDA (40 nM) was injected into the subretinal cavity of wild-type C57BL/6 mice with the same volume of PBS injected as control. At 24 h after NMDA injection, RPCs pre-incubated with exosomes containing miR-449a inhibitor or NC were digested and labeled with DiI. Then RPCs were subretinally injected with final volume of 2 μL. RD10 (Pde6b mutant) mice were bred and subretinal transplantations were performed on postnatal day 15 (P15). After 2 weeks, retinal tissue was collected and analyzed.

Immunohistofluorescence staining

Mouse eyeballs were placed in 4% PFA solution for 4 h at room temperature, and then were changed into 15% sucrose solution at 4°C overnight. Frozen sections (14 μm) were cut with a cryostat and mounted on gelatinized slides. Sections were incubated with primary antibodies. The secondary antibodies were Alexa Fluor 594 donkey anti-goat (1:1,000, Invitrogen), Alexa Fluor 488 donkey anti-rabbit (1:1,000, Invitrogen), and Alexa Fluor 488 donkey anti-rat (1:1,000, Invitrogen). The stained sections were visualized and imaged under a fluorescence microscope (Eclipse Ni, Nikon) or a laser scanning confocal microscope (A1R confocal microscope, Nikon). Image Pro-Plus was used for image analysis and quantification.

Electroretinogram

Electroretinogram (ERG) was performed according to the International Society for Clinical Electrophysiology of Vision (ISCEV) guidelines with full-field (Ganzfeld) stimulation and a computer system (MonPackONE, Metrovision). The mice were placed in a dark adaption box for 12 h. Mice were anesthetized by intraperitoneal injection with 0.1 mL/10g 5% chloral hydrate (Shanghai Aladdin Bio-Chem Technology, China). The pupils were dilated with compound tropicamide eye drops (5 mg/mL). Corneal anesthesia was achieved with one drop of oxybuprocaine hydrochloride (4 mg/mL; Santen Pharmaceutical, Japan). During recording, the interference of other electromagnetic signals was avoided under dim red light.

Statistics

Statistical significance was assessed by two-tailed Student's t test when experiments had two experimental groups. To determine significant differences between multiple groups, one-way ANOVA with Tukey's post test was used. *$p < 0.05$, **$p < 0.01$, ***$p < 0.001$ were considered as significant.

DATA AVAILABILITY

All relevant data are within the paper and its supplemental information files.

SUPPLEMENTAL INFORMATION

Supplemental information can be found online at https://doi.org/10.1016/j.omtn.2023.02.015.

ACKNOWLEDGMENTS

This work was supported by the Ministry of Science and Technology of China (2015AA020918), the National Natural Science Foundation of China (31471044, 31730041, 31671523), and the development fund of FMMU (2020ZTC03).

AUTHOR CONTRIBUTIONS

C.J.G. performed experiments and collected data. X.L.C., Y.F.Z., and K.Y.Y. assisted with experiments and data collection. J.H. and H.Y. helped with data analysis and manuscript editing. H.H. and M.H.Z. designed the experiments and prepared the manuscript.

DECLARATION OF INTERESTS

The authors declare no competing interests.

REFERENCES

1. Dalkara, D., Goureau, O., Marazova, K., and Sahel, J.A. (2016). Let there be light: gene and cell therapy for blindness. Hum. Gene Ther. *27*, 134–147.
2. Sorrentino, F.S., Gallenga, C.E., Bonifazzi, C., and Perri, P. (2016). A challenge to the striking genotypic heterogeneity of retinitis pigmentosa: a better understanding of the pathophysiology using the newest genetic strategies. Eye *30*, 1542–1548.
3. Mitchell, P., Liew, G., Gopinath, B., and Wong, T.Y. (2018). Age-related macular degeneration. Lancet *392*, 1147–1159.
4. Murakami, Y., Notomi, S., Hisatomi, T., Nakazawa, T., Ishibashi, T., Miller, J.W., and Vavvas, D.G. (2013). Photoreceptor cell death and rescue in retinal detachment and degenerations. Prog. Retin. Eye Res. *37*, 114–140.
5. Wright, A.F., Chakarova, C.F., Abd El-Aziz, M.M., and Bhattacharya, S.S. (2010). Photoreceptor degeneration: genetic and mechanistic dissection of a complex trait. Nat. Rev. Genet. *11*, 273–284.
6. Brzezinski, J.A., and Reh, T.A. (2015). Photoreceptor cell fate specification in vertebrates. Development *142*, 3263–3273.
7. Sahel, J.A., Marazova, K., and Audo, I. (2014). Clinical characteristics and current therapies for inherited retinal degenerations. Cold Spring Harb. Perspect. Med. *5*, a017111.
8. Singh, M.S., Park, S.S., Albini, T.A., Canto-Soler, M.V., Klassen, H., MacLaren, R.E., Takahashi, M., Nagiel, A., Schwartz, S.D., and Bharti, K. (2020). Retinal stem cell transplantation: balancing safety and potential. Prog. Retin. Eye Res. *75*, 100779.
9. Song, C.G., Zhang, Y.Z., Wu, H.N., Cao, X.L., Guo, C.J., Li, Y.Q., Zheng, M.H., and Han, H. (2018). Stem cells: a promising candidate to treat neurological disorders. Neural Regen. Res. *13*, 1294–1304.
10. Djojosubroto, M.W., and Arsenijevic, Y. (2008). Retinal stem cells: promising candidates for retina transplantation. Cell Tissue Res. *331*, 347–357.
11. Qiu, G., Seiler, M.J., Thomas, B.B., Wu, K., Radosevich, M., and Sadda, S.R. (2007). Revisiting nestin expression in retinal progenitor cells in vitro and after transplantation in vivo. Exp. Eye Res. *84*, 1047–1059.
12. Turner, D.L., and Cepko, C.L. (1987). A common progenitor for neurons and glia persists in rat retina late in development. Nature *328*, 131–136.
13. Wetts, R., and Fraser, S.E. (1988). Multipotent precursors can give rise to all major cell types of the frog retina. Science *239*, 1142–1145.
14. Klassen, H.J., Ng, T.F., Kurimoto, Y., Kirov, I., Shatos, M., Coffey, P., and Young, M.J. (2004). Multipotent retinal progenitors express developmental markers, differentiate into retinal neurons, and preserve light-mediated behavior. Invest. Ophthalmol. Vis. Sci. *45*, 4167–4173.
15. Liljekvist-Soltic, I., Olofsson, J., and Johansson, K. (2008). Progenitor cell-derived factors enhance photoreceptor survival in rat retinal explants. Brain Res. *1227*, 226–233.
16. Zou, T., Gao, L., Zeng, Y., Li, Q., Li, Y., Chen, S., Hu, X., Chen, X., Fu, C., Xu, H., and Yin, Z.Q. (2019). Organoid-derived C-Kit^{+}/SSEA4^{-} human retinal progenitor cells promote a protective retinal microenvironment during transplantation in rodents. Nat. Commun. *10*, 1205.
17. Ballios, B.G., Cooke, M.J., Donaldson, L., Coles, B.L.K., Morshead, C.M., van der Kooy, D., and Shoichet, M.S. (2015). A hyaluronan-based injectable hydrogel improves the survival and integration of stem cell progeny following transplantation. Stem Cell Rep. *4*, 1031–1045.
18. Gambardella, G., Carissimo, A., Chen, A., Cutillo, L., Nowakowski, T.J., di Bernardo, D., and Blelloch, R. (2017). The impact of microRNAs on transcriptional heterogeneity and gene co-expression across single embryonic stem cells. Nat. Commun. *8*, 14126.
19. Bartel, D.P. (2004). MicroRNAs: genomics, biogenesis, mechanism, and function. Cell *116*, 281–297.
20. Mens, M.M.J., and Ghanbari, M. (2018). Cell cycle regulation of stem cells by microRNAs. Stem Cell Rev. Rep. *14*, 309–322.
21. Hutvágner, G., and Zamore, P.D. (2002). A microRNA in a multiple-turnover RNAi enzyme complex. Science *297*, 2056–2060.
22. Gao, F., Zhang, Y.F., Zhang, Z.P., Fu, L.A., Cao, X.L., Zhang, Y.Z., Guo, C.J., Yan, X.C., Yang, Q.C., Hu, Y.Y., et al. (2017). miR-342-5p regulates neural stem cell proliferation and differentiation downstream to notch signaling in mice. Stem Cell Rep. *8*, 1032–1045.
23. Martin, A., Jones, A., Bryar, P.J., Mets, M., Weinstein, J., Zhang, G., and Laurie, N.A. (2013). MicroRNAs-449a and -449b exhibit tumor suppressive effects in retinoblastoma. Biochem. Biophys. Res. Commun. *440*, 599–603.
24. Song, R., Walentek, P., Sponer, N., Klimke, A., Lee, J.S., Dixon, G., Harland, R., Wan, Y., Lishko, P., Lize, M., et al. (2014). miR-34/449 miRNAs are required for motile ciliogenesis by repressing cp110. Nature *510*, 115–120.
25. Marcet, B., Chevalier, B., Luxardi, G., Coraux, C., Zaragosi, L.E., Cibois, M., Robbe-Sermesant, K., Jolly, T., Cardinaud, B., Moreilhon, C., et al. (2011). Control of vertebrate multiciliogenesis by miR-449 through direct repression of the Delta/Notch pathway. Nat. Cell Biol. *13*, 693–699.
26. Yao, Y., Ma, J., Xue, Y., Wang, P., Li, Z., Li, Z., Hu, Y., Shang, X., and Liu, Y. (2015). miR-449a exerts tumor-suppressive functions in human glioblastoma by targeting Myc-associated zinc-finger protein. Mol. Oncol. *9*, 640–656.
27. Sun, X., Liu, S., Chen, P., Fu, D., Hou, Y., Hu, J., Liu, Z., Jiang, Y., Cao, X., Cheng, C., et al. (2016). miR-449a inhibits colorectal cancer progression by targeting SATB2. Oncotarget *8*, 100975–100988.
28. Wildung, M., Esser, T.U., Grausam, K.B., Wiedwald, C., Volceanov-Hahn, L., Riedel, D., Beuermann, S., Li, L., Zylla, J., Guenther, A.K., et al. (2019). Transcription factor TAp73 and microRNA-449 complement each other to support multiciliogenesis. Cell Death Differ. *26*, 2740–2757.
29. Fededa, J.P., Esk, C., Mierzwa, B., Stanyte, R., Yuan, S., Zheng, H., Ebnet, K., Yan, W., Knoblich, J.A., and Gerlich, D.W. (2016). MicroRNA-34/449 controls mitotic spindle orientation during mammalian cortex development. EMBO J. *35*, 2386–2398.
30. Nikonov, S.S., Brown, B.M., Davis, J.A., Zuniga, F.I., Bragin, A., Pugh, E.N., Jr., and Craft, C.M. (2008). Mouse cones require an arrestin for normal inactivation of phototransduction. Neuron *59*, 462–474.
31. Zheng, M.H., Shi, M., Pei, Z., Gao, F., Han, H., and Ding, Y.Q. (2009). The transcription factor RBP-J is essential for retinal cell differentiation and lamination. Mol. Brain *2*, 38.
32. Jadhav, A.P., Cho, S.H., and Cepko, C.L. (2006). Notch activity permits retinal cells to progress through multiple progenitor states and acquire a stem cell property. Proc. Natl. Acad. Sci. USA *103*, 18998–19003.
33. Zheng, M., Zhang, Z., Zhao, X., Ding, Y., and Han, H. (2010). The Notch signaling pathway in retinal dysplasia and retina vascular homeostasis. J. Genet. Genom. *37*, 573–582.
34. Mills, E.A., and Goldman, D. (2017). The regulation of notch signaling in retinal development and regeneration. Curr. Pathobiol. Rep. *5*, 323–331.
35. Zhang, Y.Z., Liu, F., Song, C.G., Cao, X.L., Zhang, Y.F., Wu, H.N., Guo, C.J., Li, Y.Q., Zheng, Q.J., Zheng, M.H., and Han, H. (2018). Exosomes derived from human umbilical vein endothelial cells promote neural stem cell expansion while maintain their stemness in culture. Biochem. Biophys. Res. Commun. *495*, 892–898.
36. Ueki, Y., Wilken, M.S., Cox, K.E., Chipman, L., Jorstad, N., Sternhagen, K., Simic, M., Ullom, K., Nakafuku, M., and Reh, T.A. (2015). Transgenic expression of the

proneural transcription factor Ascl1 in Müller glia stimulates retinal regeneration in young mice. Proc. Natl. Acad. Sci. USA *112*, 13717–13722.

37. Chang, B., Hawes, N.L., Pardue, M.T., German, A.M., Hurd, R.E., Davisson, M.T., Nusinowitz, S., Rengarajan, K., Boyd, A.P., Sidney, S.S., et al. (2007). Two mouse retinal degenerations caused by missense mutations in the beta-subunit of rod cGMP phosphodiesterase gene. Vis. Res. *47*, 624–633.

38. Baranov, P.Y., Tucker, B.A., and Young, M.J. (2014). Low-oxygen culture conditions extend the multipotent properties of human retinal progenitor cells. Tissue Eng. Part A *20*, 1465–1475.

39. Mori, M.A., Ludwig, R.G., Garcia-Martin, R., Brandão, B.B., and Kahn, C.R. (2019). Extracellular mirnas: from biomarkers to mediators of physiology and disease. Cell Metab. *30*, 656–673.

40. Liljekvist-Larsson, I., and Johansson, K. (2005). Retinal neurospheres prepared as tissue for transplantation. Brain Res. Dev. Brain Res. *160*, 194–202.

41. Shechter, R., Ronen, A., Rolls, A., London, A., Bakalash, S., Young, M.J., and Schwartz, M. (2008). Toll-like receptor 4 restricts retinal progenitor cell proliferation. J. Cell Biol. *183*, 393–400.

42. Kholodenko, R., Kholodenko, I., Sorokin, V., Tolmazova, A., Sazonova, O., and Buzdin, A. (2007). Anti-apoptotic effect of retinoic acid on retinal progenitor cells mediated by a protein kinase A-dependent mechanism. Cell Res. *17*, 151–162.

43. Zhang, X., Zhang, X., Hu, S., Zheng, M., Zhang, J., Zhao, J., Zhang, X., Yan, B., Jia, L., Zhao, J., et al. (2017). Identification of miRNA-7 by genome-wide analysis as a critical sensitizer for TRAIL-induced apoptosis in glioblastoma cells. Nucleic Acids Res. *45*, 5930–5944.